SARS-CoV-2 under an elimination strategy in Hong Kong

Haogao Gu[1]†, Ruopeng Xie[1,2]†, Dillon C. Adam[1]†, Joseph L.-H. Tsui[1]†, Daniel K. Chu[1]†, Lydia D.J. Chang[1], Sammi S.Y. Cheuk[1], Shreya Gurung[1], Pavithra Krishnan[1], Daisy Y.M. Ng[1], Gigi Y.Z. Liu[1], Carrie K.C. Wan[1], Kimberly M. Edwards[1,2], Kathy S.M. Leung[1,3], Joseph T. Wu[1,3], Dominic N.C. Tsang[4], Gabriel M. Leung[1,3], Benjamin J. Cowling[1,3], Malik Peiris[1,2,5], Tommy T.Y. Lam[1,3,5], Vijaykrishna Dhanasekaran[1,2*]‡, Leo L.M. Poon[1,2,5*]‡

Affiliations:

[1]School of Public Health, LKS Faculty of Medicine, The University of Hong Kong, Hong Kong, China.

[2]HKU-Pasteur Research Pole, School of Public Health, LKS Faculty of Medicine, The University of Hong Kong, Hong Kong, China

[3]Laboratory of Data Discovery for Health, Hong Kong Science and Technology Park, Hong Kong, China

[4]Centre for Health Protection, Department of Health, The Government of Hong Kong Special Administrative Region, Hong Kong, China

[5]Centre for Immunology & Infection, Hong Kong Science and Technology Park, Hong Kong, China

†These authors contributed equally to this work;

‡These senior authors contributed equally to this work;

*Corresponding author. Email: veej@hku.hk, llmpoon@hku.hk.

Abstract: Hong Kong utilized an elimination strategy with intermittent use of public health and social measures and increasingly stringent travel regulations to control SARS-CoV-2 transmission. By analyzing >1700 genome sequences representing 17% of confirmed cases from 23-January-2020 to 26-January-2021, we reveal the effects of fluctuating control measures on the evolution and epidemiology of SARS-CoV-2 lineages in Hong Kong. Despite numerous importations, only three introductions were responsible for 90% of locally-acquired cases, two of which circulated cryptically for weeks while less stringent measures were in place. We found that SARS-CoV-2 within-host diversity was most similar among transmission pairs and epidemiological clusters due to a strong transmission bottleneck through which similar genetic background generates similar within-host diversity.

One sentence summary: Out of the 170 detected introductions of SARS-CoV-2 in Hong Kong during 2020, three introductions caused 90% of community cases.

Severe acute respiratory coronavirus 2 (SARS-CoV-2) emerged in late 2019 (*1*) and has caused over 170 million confirmed cases and over three million deaths worldwide (as of 1-July-2021) (*2*). Heterogeneity in disease severity (*3-5*) and high virus transmission rates (*6, 7*) necessitated extensive and diverse control strategies, which achieved varied degrees of success. Hong Kong (population 7.5 million) is among the few regions that have been relatively successful in prevention and control of community transmission using an elimination strategy (*8*), with intermittent public health and social measures combined with strict isolation of cases and quarantine of close contacts in designed facilities (*9, 10*). Increasingly stringent travel regulations have been implemented to limit importation of infections (**Fig. 1**). As of 1-July-2021, 11,855 laboratory confirmed cases have been detected resulting in 210 deaths. Using contact tracing data from January to April 2020 (waves one and two) we have shown that sustained community transmission in Hong Kong was largely driven by superspreading events, with 80% of community infection caused by 20% of cases (*10*). However, two large outbreaks have occurred in Hong Kong since this period (waves three and four). Here, we show that the three major surges in infections that occurred during waves two to four were the result of only three virus introductions (PANGO lineages (*11*) B.3, B.1.1.63, and B.1.36.27) out of a total of 170 captured through genome sequencing, resulting in 90.0% of the confirmed cases of SARS-CoV-2 observed in the community in Hong Kong. Using genomic data generated from travel-related (n=186) and community cases (n=1,713) during all four waves of the pandemic, comprising 51.4%, 21.1%, 23.6% and 13.7% of all cases in the corresponding period, respectively (**figs. S1**, **S2** and **S3**, **tables S1** and **S2**), we discuss the effects of intermittent use of public health and social measures on the evolution and epidemiology of SARS-CoV-2 in Hong Kong.

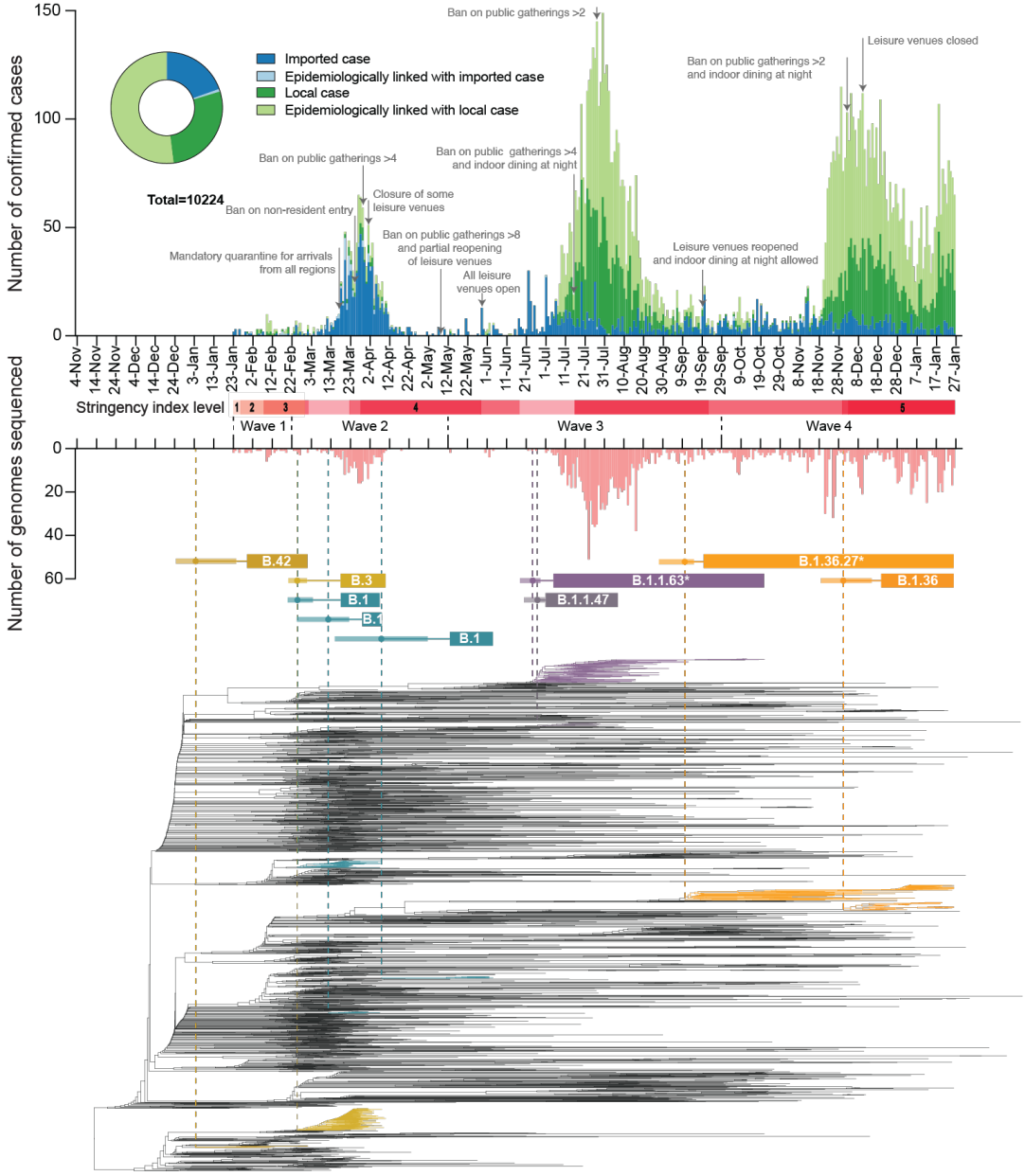

Fig. 1 Epidemiological summary and time-scaled phylogeny of SARS-CoV-2 in Hong Kong. The number of genomes sequenced in this study is shown below in light red. Time-scaled phylogeny of SARS-CoV-2 genomes from Hong Kong, in which lineages HK-wave3 and HK-wave4A were subsampled to 100 and 65 sequences, showing B.1.1.63* and B.1.36.27*, respectively. *denotes the real clade contains more than one PANGO lineage (see **Materials and Methods** and **table S4**). Red shaded bars below the timeline delineate five stringency levels of control measures in Hong Kong based on the Oxford COVID-19 Government response tracker (level 1: <40; level 2 : 40–50; level 3: 50–60; level 4: 60–70; level 5: >70) (*12*).

Introductions, local spread, and delayed detection during waves one and two

During wave one (23-January-2020 to 22-February-2020), laboratory-confirmed cases did not exceed 10 per day (**Fig. 1** and **table S1**) and were comprised of both travel-related (n=17/70, 24.3%) and community-acquired cases (n=53/70, 75.7%). The first recognised introduction was detected on 30-January-2020 among a family cluster where the index case had returned from Wuhan, China on 22-January, while the first community case without a known source (travel history or contact with a confirmed case) was also reported on 30-January. However, among two of the earliest locally circulating lineages, time-scaled phylogenetic analysis estimated a median time to most recent common ancestor (tMRCA) of 30-December-2019 (95% Highest Posterior Density Interval (HPD) 24-December-2019 – 1-January-2020) indicating direct ancestry to cases circulating prior to the earliest recognised introductions (**Fig. 2A**). Critically, these lineages had no recognised epidemiological or phylogenetic link to all other imported cases identified and sampled at the time, indicating that the source of these lineages initially entered Hong Kong undetected and triggered sustained community transmission during the first wave. Though the tMRCA indicates introduction could have occurred as early as 24-December-2019, which would represent one of earliest examples of transmission outside mainland China, it cannot be proven as the lineage diversity observed may have first accumulated in mainland China and subsequently been imported closer to the detection of the earliest cases.

As SARS-CoV-2 was declared a global pandemic on 11-March-2020, Hong Kong experienced a substantial rise in travel-related cases (n=705/978, 72.1%, **Fig. 1** and **table S1**) concomitant with large epidemics internationally (wave two). Introductions occurred mostly from outside of China (**fig. S4**), with a moderate increase observed in community cases (n=273/978, 27.9%). Again, the inferred common ancestry of community-linked lineages indicated circulation prior to or during early March 2020 (tMRCA), indicating a pattern of prolonged cryptic transmission that preceded increases in community spread (**Fig. 2A**). The largest of these local lineages comprised 92 genomes or 38.0% (n=92/242) of all sampled genomes during wave two and was classified as PANGO lineage B.3. This lineage was associated with a superspreading event from which contact tracing identified 106 community cases. Genomic analysis linked an additional 16 sporadic community cases, increasing the total inferred cluster size to 122 or 46.2% (n=122/326) of community cases during waves one and two.

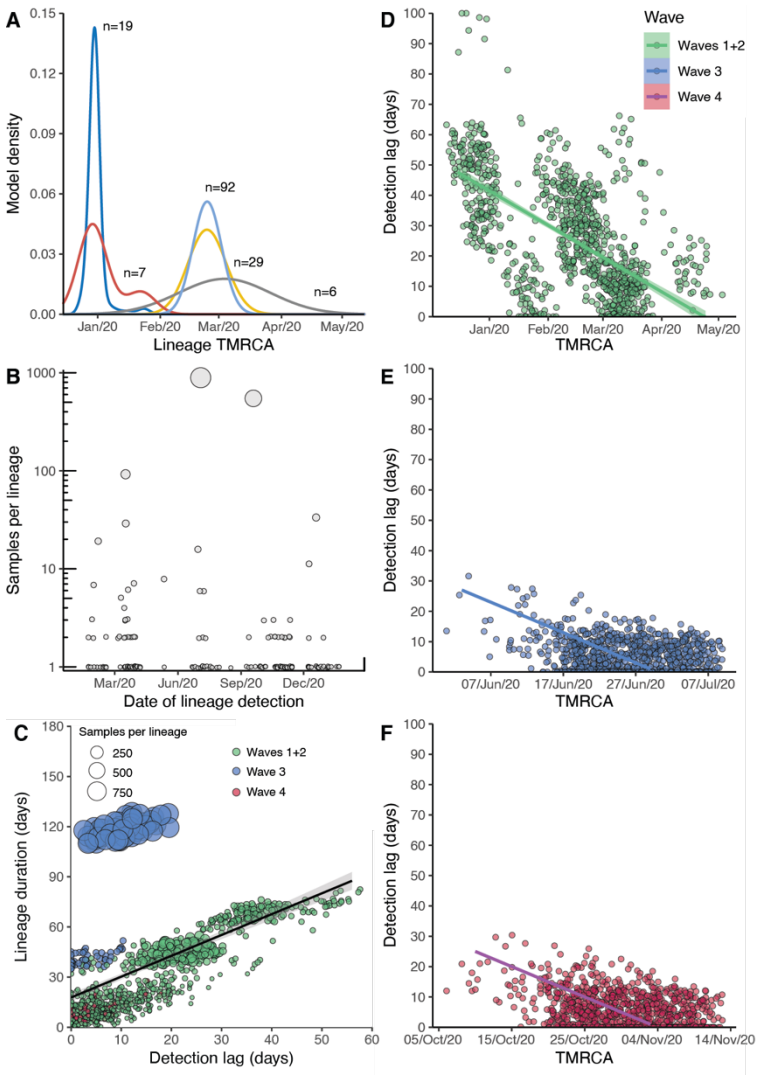

Fig. 2 Descriptive and temporal dynamics of SARS-CoV-2 lineages in Hong Kong. (A) Time to most recent common ancestor (tMRCA) among the five earliest locally circulating lineages of SARS-CoV-2 introduced into Hong Kong. **(B)** Number of SARS-CoV-2 genomic samples per lineage identified over time. Lineage size is ordered on a log10 scale, and plotted by the earliest confirmation date among the lineages. **(C)** Correlation between the detection lag of locally circulating lineages and the final lineage duration. Points represent a random sample of 1,000 lineages from a Bayesian posterior tree distribution (n=8,000). **(D:E)** Detection lag over time as a function of tMRCA across three epidemic periods **(D)** waves one and two, **(E)** wave three, **(F)** wave four. Overall, a significant reduction in detection lag was observed over time and across each epidemic wave. Points in each panel represent a random sample of 1,000 lineages from a Bayesian posterior tree distribution (n=8,000).

Overall, during waves one and two, there were 38 lineages circulating in the community (out of a total of 61 unique imported clades). The median size for non-singleton local lineages was six cases, and the median duration of circulation was 10.5 days. Among local lineages without traced contact to an imported case, the median delay in lineage detection (time between lineage tMRCA and confirmation of the first detected case) was 25 days, though this was noticeably higher in January (median = 31 days), before significantly improving to eight days by early May 2020, likely related to early delays and subsequent improvements in case detection (Spearman's test, rho (ρ) = -0.49, $p < 0.001$, **Fig. 2D**).

Travel measures and the suppression of overseas introductions

Following a peak of infections during 16–27 March 2020 (wave two; **Fig. 1** and **table S1**), a rapid decline occurred as travel and community restrictions were expanded to include mandatory quarantine on arrival with strengthened testing, restrictions on non-resident entry, school closures, adjusted work arrangements, and bans on public gatherings (*13*). Travel restrictions began as early as 26-January-2020. First, all non-residents that visited Hubei province within two weeks were barred entry into Hong Kong. This was followed by a mandate for compulsory quarantine of passenger arrivals from regions affected with SARS-CoV-2, extending from mainland China to South Korea, Iran, Italy, and the Schengen region, and culminating in the barring of entry of non-residents during the peak of wave two in March. No community cases were reported from mid-April to 12-May-2020, and community measures were gradually relaxed to allow public gatherings of at most eight (from four) people with restricted opening of leisure venues (**Fig. 1**). Based on the Oxford COVID-19 Government response tracker (*12*), stringency of control measures reduced from level 4 to level 2 during this period (**Fig. 1**).

Reintroductions and local surge during waves three and four

The first large SARS-CoV-2 outbreak in Hong Kong occurred from July to September 2020 (wave three), resulting in >4,000 cases (**table S1**). With a predominant number of cases in the community (n=3,385/4,032, 84.0%), this third epidemic wave was preceded by a period of increased detection of travel-related cases during July 2020 (similar to waves one and two, **Fig. 2B**). While importations during wave two were predominantly from Europe, subsequent cases were mostly from Asia (**fig. S4**, **table S3** and **data S1**). The number of laboratory-confirmed

cases continued to rise, reaching a peak of >120 cases per day in late July (**Fig. 1**). Following the implementation of increasingly stringent public health and social distancing measures, the local epidemic subsided in September. However, beginning in early November a second resurgence (termed wave four) occurred, resulting in >6000 additional cases. Wave four peaked in December 2020 and slowly declined towards zero daily cases by April 2021.

Sequencing identified 170 virus lineages belonging to 71 PANGO lineages in Hong Kong within one year (**Fig. 2** and **data S2**). However, 87.0% of those lineages were detected only in travel-related cases or one community case, and no variants of concern were detected in the community during waves three and four. Notably, a single introduction belonging to lineage B.1.1.63 resulted in over 90.0% of genomes sampled during wave three (92.4%, 881/953), forming a HK-wave3 clade (n=902) (also see **fig. S1** and **table S4**). However, the earliest imported cases of the HK-wave3 clade were not sampled, indicating cryptic transmission prior to detection. In a similar trend, two lineages led to most of the fourth wave cases: over 74% genomes (552/704) formed one clade (HK-wave4A, B.1.36.27, **table S4**), and 4.7% (33/704) formed another (HK-wave4B, B.1.36).

By comparing the tMRCA of local non-singleton clusters in Hong Kong (n=7, 6.4% (7/109)) (**Fig. 2** and **data S3**), we identified two introductions (HK-wave3 and HK-wave4A) that circulated in the community for 108 and 128 days, respectively. The delay in detection of local non-singleton lineages remained low during waves three and four (mean=2.9 days, 95% HPD 0 - 13 days) (**Fig. 2E**, **F**), with a detection delay of 11 and 10 days for the two large clades, HK-wave3 and HK-wave4A, respectively (**data S3**). A negative correlation between delay over time from wave one to wave four (Spearman's test, rho (ρ) = -0.72, $p < 0.001$), indicates improvements in identifying cases during 2020 (**Figs. 2D**, **E** and **F**). Interestingly, the cryptic circulation of HK-wave3 occurred during periods of reduced stringency (level 2), however HK-wave4A introduction occurred during the late stages of wave three when stringency level 4 was enacted, and continued to circulate cryptically when stringency level was reduced to level 2 on presumed suppression of the second wave. Similarly, HK-wave4B introduction occurred during relatively stringent level 4 (**Fig. 1**), while a significant positive correlation between increasing lag in lineage detection and lineage duration was observed (Spearman's test, rho (ρ) = 0.70, $p < 0.001$, **Fig. 2C**).

Contrasting patterns of epidemiology during waves three and four

To understand the effects of public health and social measures on community transmission, we characterized the two largest clades that circulated during waves three and four and identified contrasting pattens of genomic evolution and underlying transmission dynamics. HK-wave3 emerged during a period of reduced community measures (stringency level 2) and was controlled by increasing stringency to level 4. By contrast, HK-wave4A emerged under stringency level 4 and circulated cryptically during reduced level 3. Although the stringency level was rapidly raised to 5 on detection, HK-wave4A continued to circulate for several months.

The effective reproductive number (R_e) estimated using a birth-death skyline serial (BDSS) model (*14*) for 902 HK-wave3 genomes collected from all 18 districts in Hong Kong (5-July-2020 to 21-October-2020) showed that R_e was significantly higher (~3) from the tMRCA in late June or early July (mean tMRCA = 1-July-2020, 95% HPD, 26-June-2020 to 4-July-2020) until recognition of the lineage on 5-July when stringency level was 2 (**Fig. 3**), highlighting a period of rapid virus expansion when leisure venues were open and public gatherings of up to 50 people were allowed. Notably, as the control stringency was increased on 15-July (from level 2 to 4), R_e subsided to ~2 and subsequently decreased below ~1. An increasing number of cases continued to be reported among close contacts in residential care homes for the elderly or disabled, households, hospitals, dormitories and workplaces, whereas just 12.6% of the genomes were attributable to social interactions (**table S5**). Phylogenies reveal a rapid termination of transmission lineages among close contacts, leading to disappearance of all but one sub-lineage that continued to circulate with R_e >1 until extinction in October 2020. These results indicate suppression with level 4 stringency during wave three, complimented by aggressive contact tracing, resulted in the elimination of the majority of wave three transmission chains despite the intermittent rise in cases among close contacts.

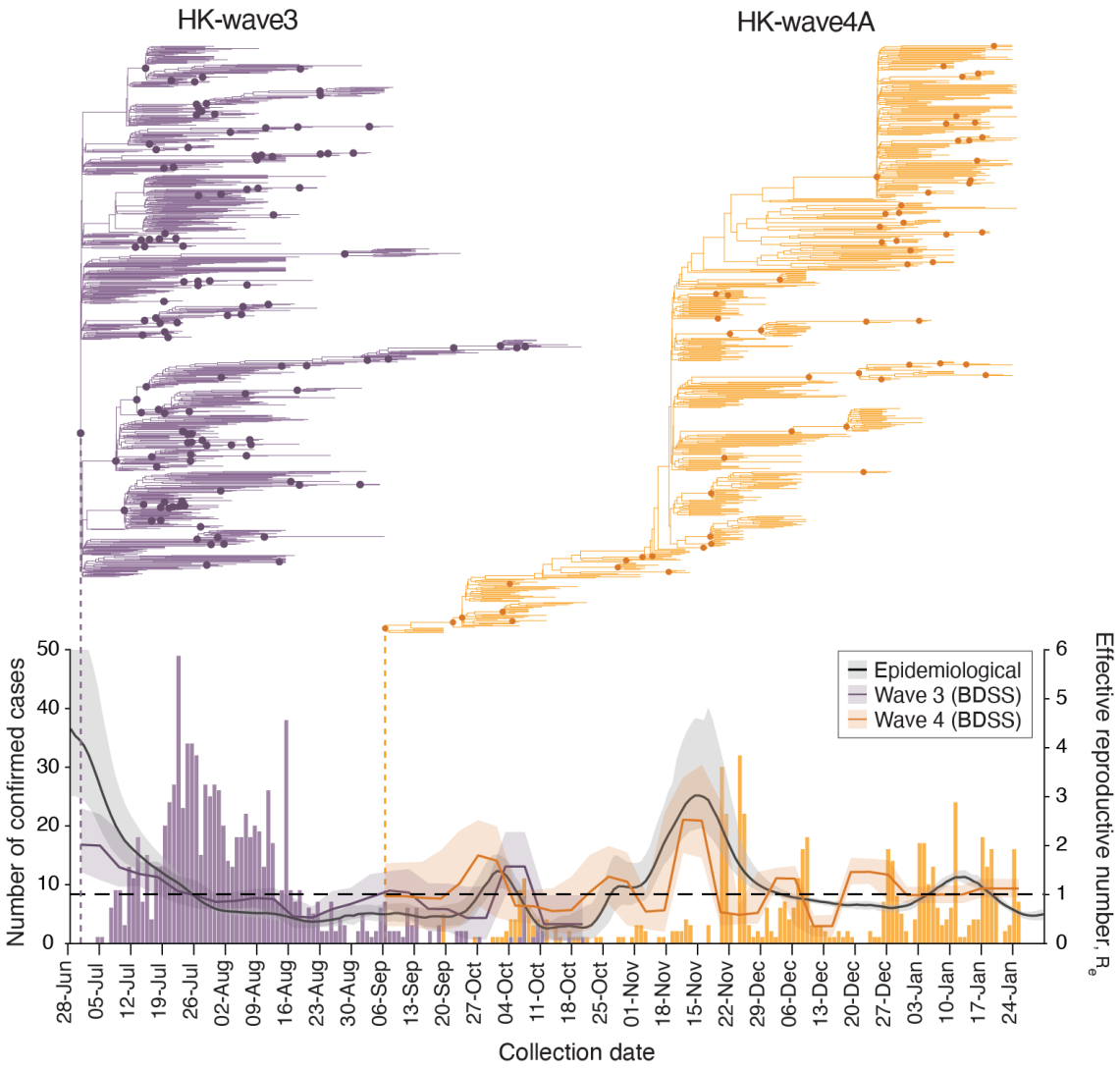

Fig. 3 Phylodynamics of waves three and four in Hong Kong. Evolutionary relationships and effective reproduction number ($R_e(t)$) of HK-wave3 (B.1.1.63) clade (purple) and HK-wave4A (B.1.36.27) clade (orange) estimated using tree-heights and sequenced incidence data. Purple and orange bars show the number of genomes by collection date. Black line shows the instantaneous effective reproduction number (R_t), estimated based on infection dates inferred from the reported dates of symptom onset (or dates of confirmation for asymptomatic cases).

HK-wave4A (mean tMRCA = 6-September-2020, 95% HPD 5–7 September-2020) continued to circulate for several months despite level 5 stringency (**Fig. 3**). In contrast to HK-wave3, a rapid expansion did not occur upon emergence. Instead, the HK-wave4A dynamics resembled the pattern of a propagated epidemic curve, with R_e increasing with each subsequent peak during

September and November, achieving a high of R_e ~3 during mid to late November; R_e fluctuated around 1 following this period. The structure of the phylogenetic tree suggests continual elimination of viral lineages with intermittent expansion coinciding with a superspreading event involving 28 dancing and singing venues in different districts of Hong Kong, resulting in a group of 732 cases epidemiologically linked to this superspreading event. Epidemiological data shows that up to 23.6% of genomes during this wave were related to social clusters (**table S5**) which is significantly higher than the HK-wave3 counterpart ($p < 0.001$, chi-square test). Human mobility levels inferred from Octopus, a smart card payment system used by >98% of the Hong Kong population aged 16 to 65 (*15*), showed adult and elderly mobility within Hong Kong resumed to pre-pandemic levels during the early stage of wave four in early to mid-November 2020 (~100% of the average level during 1–15 January 2020) (**fig. S5**). Taken together, our results suggest that community measures reduce R_e, however prolonged community measures decrease the probability of lineage termination due to fatigue arising in the population (*16, 17*).

The instantaneous effective reproductive numbers (R_t) of local cases are consistent with R_e of the two major transmission lineages during waves three and four (**Fig. 3**). During the short period of lineage co-circulation (**Fig. 3**), the relative reproductive number of HK-wave3 estimated using a relative fitness inference framework (*15*) was higher (mean = 1.28, credible interval [CrI] 0.88-1.93) when compared with HK-wave4A, though the difference in transmissibility was not significant (CI across 1.0). However, these estimates of comparative transmissibility may be affected by stochasticity, such as the occurrence of superspreading events as revealed through sequencing.

Within-host genetic variation determined by genetic background

By analyzing deep-sequence data from confirmed donor and recipient pairs using a beta-binomial statistical framework (*18*) we estimated the number of virions required to initiate infection was between one to three (**Fig. 4A**, **Materials and Methods** and **table S8**). This is consistent with data from transmission pairs estimated in UK and Austria (one to eight in UK and one to three in Austria (*19, 20*)) as well as between cats (two to five virions (*21*)), showing SARS-CoV-2 transmission bottleneck may be universally small. To understand the effects of strong transmission bottlenecks on within-host diversity, we estimated Jaccard distances between sample pairs and found that minor variants were not significantly different between established

196 transmission pairs and epidemiologically clustered samples (**Fig. 4B**) but were significantly
197 different between samples without epidemiological links. These results show that the SARS-
198 CoV-2 within-host genetic variation is non-random and determined by genomic differences (i.e.
199 consensus sequence), shedding new light on SARS-CoV-2 evolution.

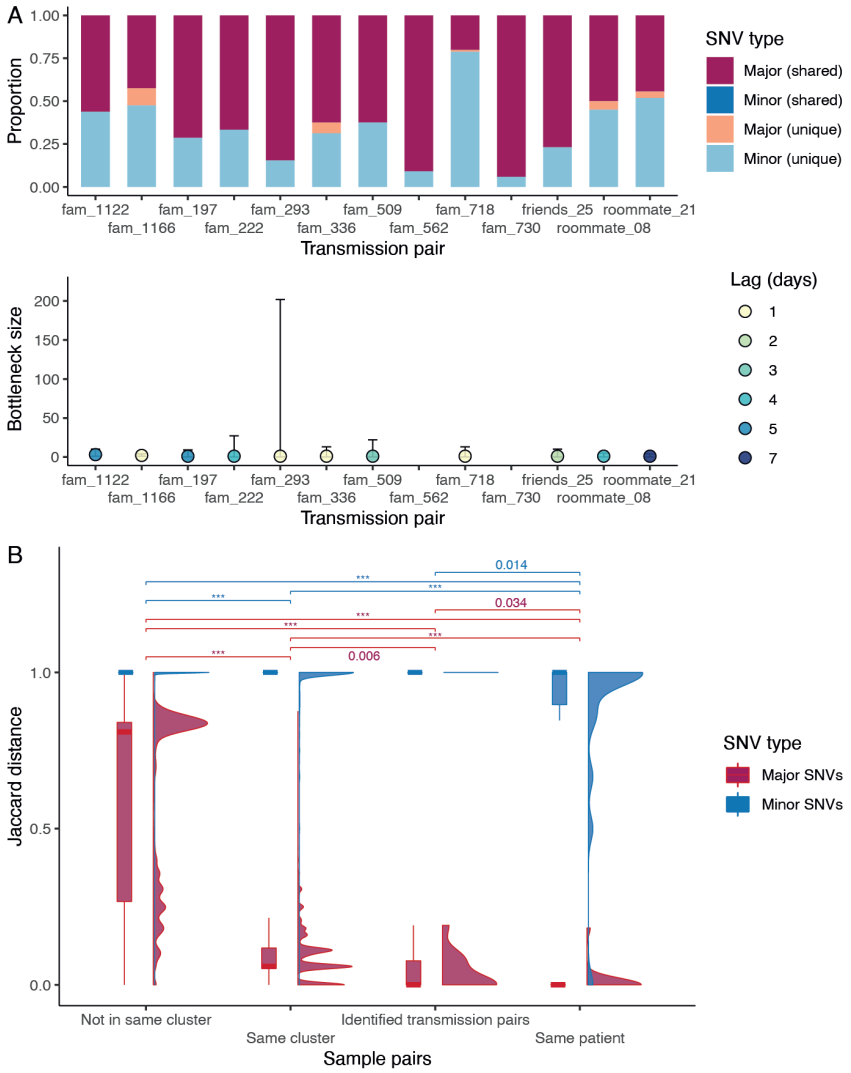

200 **Fig. 4 Transmission bottleneck and mutation profiles between cases. (A)** Proportion of
201 shared mutations and transmission bottleneck size estimations (with 95% confidence intervals)
202 between samples from established transmission pairs. The estimates for transmission pairs
203 fam_562 and fam_730 are not available due to a limited number of SNVs in the recipients'
204 samples. **(B)** Jaccard distance of the major and minor SNVs between different types of sample
205 pairs. The distribution is shown in both boxplot and density plot. The between-group differences
206 were tested by Wilcoxon tests, and p values < 0.05 are shown (p values < 0.001 are labelled as
207 ***).

Conclusions

Sequencing allowed us to investigate the introduction and circulation pattens of SARS-CoV-2 transmission lineages under the elimination strategy in Hong Kong. Border control measures averted numerous introductions, and community outbreaks were typically associated with cryptic virus circulation during less stringent periods and expansion through superspreading events. Heightened control measures eliminated most transmission chains in the local community, but the proportion of social transmission during wave four was significantly higher than that of wave three, indicating control was less effective when prolonged. Although public health and social measures were promptly lifted when community cases could be traced and controlled, new waves continued as a result of new introductions rather than resurgence of previously circulating viruses. This shows that contact tracing was efficient, but averting outbreaks from new introductions requires heightened border control and enhanced community surveillance during periods of lower control level stringency.

References

1. F. Wu *et al.*, A new coronavirus associated with human respiratory disease in China. *Nature* **579**, 265-269 (2020).
2. E. Dong, H. Du, L. Gardner, An interactive web-based dashboard to track COVID-19 in real time. *Lancet Infect Dis* **20**, 533-534 (2020).
3. R. Verity *et al.*, Estimates of the severity of coronavirus disease 2019: a model-based analysis. *Lancet Infect Dis* **20**, 669-677 (2020).
4. T. W. Russell *et al.*, Estimating the infection and case fatality ratio for coronavirus disease (COVID-19) using age-adjusted data from the outbreak on the Diamond Princess cruise ship, February 2020. *Euro Surveill* **25**, (2020).
5. J. T. Wu *et al.*, Estimating clinical severity of COVID-19 from the transmission dynamics in Wuhan, China. *Nat Med* **26**, 506-510 (2020).
6. K. Mizumoto, K. Kagaya, A. Zarebski, G. Chowell, Estimating the asymptomatic proportion of coronavirus disease 2019 (COVID-19) cases on board the Diamond Princess cruise ship, Yokohama, Japan, 2020. *Euro Surveill* **25**, (2020).
7. L. Ferretti *et al.*, Quantifying SARS-CoV-2 transmission suggests epidemic control with digital contact tracing. *Science* **368**, (2020).
8. M. G. Baker, N. Wilson, T. Blakely, Elimination could be the optimal response strategy for covid-19 and other emerging pandemic diseases. *BMJ* **371**, m4907 (2020).
9. B. J. Cowling *et al.*, Impact assessment of non-pharmaceutical interventions against coronavirus disease 2019 and influenza in Hong Kong: an observational study. *Lancet Public Health* **5**, e279-e288 (2020).
10. D. C. Adam *et al.*, Clustering and superspreading potential of SARS-CoV-2 infections in Hong Kong. *Nat Med* **26**, 1714-1719 (2020).
11. A. Rambaut *et al.*, A dynamic nomenclature proposal for SARS-CoV-2 lineages to assist genomic epidemiology. *Nat Microbiol* **5**, 1403-1407 (2020).
12. T. Hale *et al.*, A global panel database of pandemic policies (Oxford COVID-19 Government Response Tracker). *Nat Hum Behav*, (2021).
13. G. M. Leung, B. J. Cowling, J. T. Wu, From a Sprint to a Marathon in Hong Kong. *N Engl J Med* **382**, e45 (2020).
14. T. Stadler, D. Kuhnert, S. Bonhoeffer, A. J. Drummond, Birth-death skyline plot reveals temporal changes of epidemic spread in HIV and hepatitis C virus (HCV). *Proc Natl Acad Sci U S A* **110**, 228-233 (2013).
15. K. Leung, M. H. Shum, G. M. Leung, T. T. Lam, J. T. Wu, Early transmissibility assessment of the N501Y mutant strains of SARS-CoV-2 in the United Kingdom, October to November 2020. *Euro Surveill* **26**, (2021).
16. D. Zhanwei *et al.*, Pandemic fatigue impedes mitigation of COVID-19 in Hong Kong. *Research Square*, (2021).
17. L. Qiuyan *et al.*, Community Psychological And Behavioural Responses To Coronavirus Disease 2019 Over One Year Of The Pandemic In 2020 In Hong Kong. *Scientific Reports*, (2021).
18. A. Sobel Leonard, D. B. Weissman, B. Greenbaum, E. Ghedin, K. Koelle, Transmission Bottleneck Size Estimation from Pathogen Deep-Sequencing Data, with an Application to Human Influenza A Virus. *J Virol* **91**, (2017).
19. K. A. Lythgoe *et al.*, SARS-CoV-2 within-host diversity and transmission. *Science* **372**, (2021).

20. M. A. Martin, K. Koelle, Reanalysis of deep-sequencing data from Austria points towards a small SARS-COV-2 transmission bottleneck on the order of one to three virions. *bioRxiv*, 2021.2002.2022.432096 (2021).
21. K. M. Braun *et al.*, Transmission of SARS-CoV-2 in domestic cats imposes a narrow bottleneck. *PLoS Pathog* **17**, e1009373 (2021).

Acknowledgments: We gratefully acknowledge the staff from the originating laboratories responsible for obtaining the specimens and from the submitting laboratories where the genome data were generated and shared via GISAID. We thank Octopus Cards Limited for providing aggregate data of passenger numbers by public transportation means and aggregate data of transactions by retail categories for the research. We acknowledge the technical support provided by colleagues from the Centre for PanorOmic Sciences of the University of Hong Kong. We also acknowledge the Centre for Health Protection of the Department of Health for providing epidemiological data for the study. The computations were performed using research computing facilities offered by Information Technology Services, the University of Hong Kong. The funding bodies had no role in the design of the study, the collection, analysis, and interpretation of data, or writing of the manuscript.

Funding:

Health and Medical Research Fund, Food and Health Bureau of the Hong Kong SAR Government COVID190118 (LLMP)

Collaborative Research Fund of the Research Grants Council of the Hong Kong SAR Government C7123-20G (BJC)

National Institutes of Health grant U01AI151810 (LLMP)

National Institutes of Health grant HHSN272201400006C (JSMP, LLMP, BJC, DV)

National Institutes of Health grant 75N93021C00016 (JSMP, LLMP, DV)

Author contributions:

Study Design: LLMP, DV

Data curation: HG, RX, DCA, DNCT, KME

Genome sequencing group: LLMP, JSMP, DKC, HG, LDJC, SSYC, SG, PK, DYMN, GYZL, CKCW

Phylodynamic analysis group: DV, TTYL, DCA, HG, RX, KSML, JL-HT

Visualization: HG, RX, DCA, TTYL, DV

Supervision: LLMP, DV, BJC, JSMP, TTYL, JTKW

Writing – original draft preparation: DV, RX, DCA, HG, TTYL

Writing – review & editing: LLMP, DV, DCA, TTYL, KME, JSMP, BJC, GML

Competing interests: BJC has consulted for Roche, Sanofi Pasteur, GSK, AstraZeneca and Moderna. The authors declare no other competing interests.

Data and materials availability: Hong Kong SARS-CoV-2 genome sequences and associated metadata is deposited at gisaid.org. All anonymized data, sequence accession numbers, code, and analysis files are available in supplementary materials and in GitHub repository (https://github.com/hku-sph-covid-19-genomics-consortium/hk-sars-cov-2-genomic-epidemiology).

Supplementary Materials

Materials and Methods

Figs. S1 – S8

Tables S1 – S10

Supplementary references (*22 – 45*)

Data S1 – S4

Supplementary Materials

Materials and Methods

SARS-CoV-2 data from Hong Kong

De-identified saliva or nasopharyngeal samples positive for SARS-CoV-2 by real time-polymerase chain reaction (RT-PCR), along with epidemiological information including onset date, report date and contact history for individual cases were obtained from the Centre for Health Protection, Hong Kong.

Genomic sequencing of SARS-CoV-2

A total of 1,753 laboratory-confirmed samples were collected from 1,733 RT-PCR confirmed cases from 22-June-2020 to 26-January-2021. Virus genome was reverse transcribed with primers targeting different regions of the viral genome, published in (*22*). The synthesized cDNA was then subjected to multiple overlapping 2kb PCRs for full-genome amplification. PCR amplicons obtained from the same specimen were pooled and sequenced using Nova sequencing platform (PE150, Illumina). Sequencing library was prepared by Nextera XT. The base calling of raw read signal and demultiplexing of reads by different samples were performed using Bcl2Fastq (Illumina). A reference-based re-sequencing strategy was applied in analyzing the NGS data. Specifically, the raw FASTQ reads were assembled and mapped to the SARS-CoV-2 reference genome (Wuhan-Hu-1, GenBank: MN908947.3) using BWA mem2 (v.2.0pre2) (*23*). The consensus sequences for each sample were called as dominant bases at each position by samtools mpileup (v.1.11) (*24*) with minimum depth of 100 reads. Samples less than 27kb in length (excluding gaps) were excluded from downstream analysis. The head and tail 100nt bases of all generated consensus sequences were masked. We also masked another 10 sites located in PCR primer binding regions and observed to be variant (≥ 3% allele frequency) in 1% or more HK samples (**table S9**). The same masking strategy was also applied in phylodynamics analysis, variant calling, and bottleneck estimation. The average sequencing depth (number of mapped reads) at each nucleotide position that was retained ranged from ~10,000 to ~100,000 (**fig. S6**).

There were 16 patients from which samples were collected or sequenced at multiple time points. Twelve samples from 6 patients were sequenced in duplicate, and 21 samples from 10 patients were collected sequentially. One representative sample for each of the 16 patients was selected based on genome coverage and average sequencing depth. In total, 1,601 representative samples met quality control standards. All 1,601 consensus sequences from Hong Kong, as well as 298 additional consensus sequences from the first two waves were included in the phylogenetic analysis. Sequences from regions outside Hong Kong were retrieved from the GISAID database (total 399,124 sequences, accessed 16-February-2021, detailed accession numbers and acknowledgement information in **data S4**).

Phylogenetic analysis of SARS-CoV-2 in Hong Kong

Hong Kong sequences were analysed with a global SARS-CoV-2 genome alignment obtained from GISAID (accessed 16-February-2021). For each Hong Kong sequence, the three most similar global sequences (evaluated by p distance excluding gaps, n = 385), as well as the earliest sampled sequence (n = 1,279) from each PANGO lineage (accessed 07-May-2021) (*11*) were selected. After removing repetitive sequences and trimming masked sites, data quality was evaluated using a root-to-tip regression analysis in TempEst (v.1.5.3) (*25*), resulting in a final set of 3,437 sequences. Maximum likelihood (ML) phylogenies were estimated using IQ-TREE (v.2) (*26*), employing the best-fit nucleotide substitution model with Wuhan-Hu-1 (GenBank:

MN908947.3) as the outgroup and dated by least square dating (LSD2) (*27*). Branch support was estimated using ultrafast bootstrap approximation (UFBoot) and SH-like approximate likelihood ratio test (SH-aLRT), and for nodes of interest with <50% support, we examined their stability through multiple iterative runs using the best-fit nucleotide substitution model. Internal branches with zero-length were preserved for dating by setting parameter *l* as -1. SARS-CoV-2 sequences from Hong Kong were classified based on the dynamic PANGO nomenclature system (https://github.com/cov-lineages/pangolin, v.2.3.9, 23-April-2021) (*11*) and confirmed using a ML analysis.

Phylodynamics of Hong Kong waves

To identify monophyletic clusters of SARS-CoV-2 lineages in Hong Kong, Bayesian molecular clock phylogenetic analysis pipeline proposed by Plessis *et al.* (*28*) were implemented. In this study, the data tree and starting tree were applied to a ML tree generated by IQ-TREE (v.2) (*26*) with LSD2 (*27*). Time-scaled phylogenies were generated using the strict clock model with 0.001 substitutions per site per year which is within 95% credible interval of SARS-CoV-2 temporal signal (*29*), the Skygrid model (*30*) with 61 grid points and a Laplace root-height prior with mean equal to the dated-ML tree estimated by IQ-TREE (v.2) (*26*) and scale is set to 20% of mean. To improve computational efficiency, two largest local monophyletic clades in wave three (HK-wave3, n = 902) and wave four (HK-wave4A, n = 552) from ML tree were subsampled to 100 and 65 sequences by 5 earliest cases, 5 latest cases and 10% of the remaining randomly selected, respectively. We ran nine MCMC chains of 100 million, sampling every 1,000 steps and discarding 10% as burn-in. As there are no collapsed internal branches in this study, only uncertainty in branch durations were estimated by MCMC. From the approach described in Geoghegan *et al.* (*31*), we used the R package "NELSI" (*32*) to identify classify all monophyletic lineages, including singletons, and to estimate the delay in lineage detection following importation as well as the duration of circulation, given a set of 8,000 posterior trees. It's notable that there are two global sequences from Japan (EPI_ISL_591420 and EPI_ISL_721612) present in the HK-wave3 clade. However, these two Japan cases had travel history to the Philippines (similar to the early HK-wave3 imported cases), and were quarantined when landed in Japan, suggesting that they are unlikely to have caused an introduction in Hong Kong. These two cases were therefore excluded when defining the HK-wave3 clade.

For all samples of HK-wave3 and HK-wave4A, we used the birth-death skyline serial (BDSS) model (*14*) implemented in BEAST (v.2.6.3) (*33*) to infer the time of origin (tOrigin), time of most recent common ancestor (tMRCA) and temporal variations (piecewise fashion over 12-15 equidistant intervals) in the effective reproductive number denoted as R_t. A non-informative prior for tOrigin was used with a the lower bound set to 1-January-2020. The HKY + G4 nucleotide substitution model and an uncorrelated relaxed molecular clock model with lognormal rate distribution (UCLN) (*34*) were used. The sampling proportion was given a uniform distribution as prior with the upper bound at the empirical ratio of the number of sequences to the number of reported cases. MCMC chains were run for 600 million and 800 million steps and sampled every 2,000 and 10,000 steps for the lineages HK-wave3 (B.1.1.63) and HK-wave4A (B.1.36.27) respectively, with the initial 10% discarded as burn-in. This resulted in a final total of 270,000 and 72,000 sampled states. Mixing of the MCMC chain was inspected using Tracer (v1.7.1) (*35*) to ensure an effective sample size (ESS) of >200 for each parameter. Change in the effective reproductive number over time after the estimated tMRCA was plotted using R package "bdskytools" (https://github.com/laduplessis/bdskytools). Since by definition there are no sequences between tMRCA and the estimated tOrigin, the effective

reproductive number (R_e) was assumed to remain constant in this period. This assumption was incorporated in the default birth-death model using the package TreeSlicer in BEAST2.

Human mobility in Hong Kong using Octopus data

We used digital transactions made on Octopus cards, ubiquitously used by the Hong Kong population for daily public transport and small retail payments (https://www.octopus.com.hk/tc/consumer/index.html), to obtain changes in mobility during 2020–2021 among cards classified as children, students, adults and elderly (**fig. S5**).

Analysis of within-host genetic variation and transmission bottleneck

Deep sequencing SARS-CoV-2 samples in the United Kingdom and Austria has shown that the within-host genetic diversity (iSNV) is low with a narrow bottleneck during transmission (*19, 20*). Within-host genetic variation (iSNV) depends on intra-host virus evolution and transmission bottleneck size. To determine the baseline similarity of within-host genetic diversity, we prepared two sets of samples as controls: (a) six samples were sequenced in duplicate to account for uncertainty arising from sequencing; and (b) twenty-one samples collected from ten individuals. To examine the dynamics of mutations related to transmission events, we identified 13 transmission pairs (donor and recipient) that were directly linked with symptom onset varying by 1 to 7 days.

Single nucleotide variants (SNVs) in deep-sequence data were identified using three different variant callers, freebayes (v.1.3.2) (*36*), VarDict (v.1.82) (*37*) and LoFreq (v.2.15) (*38*). To attain a robust variant calling result, only SNVs detected by at least two different variant callers were analyzed in this study (*8*). SNVs with a minimum depth of 100 reads, minimum frequency of 3%, and detected by at least two different variant callers were retained for further analysis. Parameters and scripts for this pipeline are described in https://github.com/hku-sph-covid-19-genomics-consortium/hk-sars-cov-2-genomic-epidemiology. Gene annotations of the SNVs were based on **table S10**. To understand the uncertainty in iSNV due to the sequencing protocol, we sequenced six samples in duplicate. While detection of major variants (consensus) was consistent, detection of iSNVs may vary between sequencing runs. For example, while iSNVs of case 10 were shared between sequencing runs, iSNVs of case 15 were mutually exclusive (**fig. S7**). Similarly, when comparing iSNV of 21 samples collected from 10 individuals, major variants in samples from the same patient remained identical but their iSNVs varied. A similar pattern was observed in transmission pairs, where most of the major variants are shared but some of the minor variants are unique (**Fig. 4A**), which can be explained by a narrow transmission bottleneck.

The statistical framework for estimating the transmission bottleneck size between identified transmission pairs was introduced in (*18*). It was based on a beta-binomial method which models the number of transmitted virions from donor to the recipient. Because of the high sequencing depth of the data, the minimum variant calling threshold was set to 0.03 with a minimum depth of 100 reads. Bottleneck size estimates were calculated by maximum likelihood analysis comparing the allele frequency of variants passing threshold between samples. The 95% confidence intervals were calculated using a likelihood ratio test. To identify similarity of SNVs between samples we used the Jaccard distance, defined as one minus the proportion of intersection between two samples divided by the proportion of their union.

$$Jaccard(A,B) = 1 - \frac{|A \cap B|}{|A \cup B|}$$

SARS-Cov-2 sequences from Hong Kong contained within-patient variation in 12,859 sites of the genome when compared to the SARS-CoV-2 reference strain Wuhan-Hu-1 (GenBank: MN908947.3). 37.2% of the sites (n=4,779) contained mutations in more than one sample. High frequency of variation (in >100 Hong Kong sequences) was observed in 30 sites (**table S6**). The spectrum of allele frequencies (**fig. S8**) showed that over 90% of the variants had allele frequency ≥95% or ≤10%. Mutation hotspots were detected in four sites of the genome with a greater frequency of intra-host single nucleotide variation (iSNVs). These mutations were sporadically distributed across the phylogeny and present in ~20 sequences from the GISAID data, which may suggest potential homoplasy. We observed two variants unique to Hong Kong, C5812T and G25785T, which were detected in separate phylogenetic clusters of local Hong Kong cases. The C5812T mutation was identified in two sperate clusters in the fourth wave. While the C5812T mutation in one cluster likely descended from a local ancestral case, the mutation in the earlier cluster may have been imported. Similarly, G25785T was found in both the third and fourth waves, and mutations in at least one cluster likely originated from local cases. Some of the low frequency SNVs (frequency <5%, shown in the low peaks to the bottom of **fig. S8** and **table S7**) commonly occurred in global context. For example, the G28883C (G205R in nucleocapsid) and C22227T (A665V in spike) mutations were found in 38.09% and 21.49% of the global cases, however they were only seen in 1.56% and 0.7% of the Hong Kong cases respectively.

Estimation of the instantaneous effective reproductive number (R_t)

The instantaneous effective reproduction number R_t is defined as the average number of secondary cases generated by cases on day t. If $R_t > 1$ the epidemic is expanding at time t, whereas $R_t < 1$ indicates that the epidemic size is shrinking at time t. The transmissibility of imported and local cases was expected to be very different because intensive non-pharmaceutical interventions had been imposed on travelers arriving from COVID-19 affected regions since January 2020. Hence, we only included cases from the following three categories into the computation of R_t, i.e., local case and epidemiologically linked with local cases defined by the Centre for Health Protection (CHP, https://www.coronavirus.gov.hk/eng/index.html).

Since the epidemic curves provided by CHP were based on the dates of symptom onset or dates of confirmation, we used a deconvolution-based method to reconstruct the COVID-19 epidemic curves by dates of infection (*39, 40*). We assumed that the incubation period was Gamma with mean and standard deviation of 6.5 and 2.6 days (*41*), and that the distribution of the time between symptom onset and case confirmation was Gamma with mean and standard deviation of 4.3 and 3.2 days. For asymptomatic cases, we assumed they shared the same distribution of the time between infection and case confirmation with the symptomatic cases. We then computed R_t for local cases only from the respective epidemic curves using the "*EpiEstim*" (*42*) R package (**Fig. 3**).

Estimation of the relative reproductive number of HK-wave3 compared with HK-wave4A

We defined the comparative transmissibility of any two lineages as the relative reproductive number, i.e., the ratio of their basic reproductive numbers. We extended a previous competition transmission model (*43, 44*) of two viruses and applied the fitness inference framework to the sequence data collected in Hong Kong during the cocirculation period of HK-wave3 and HK-wave4A clades (between 19-September and 21-October-2020, **Fig. 3**). We assumed the two clades shared the same generation time distribution which can be approximated by the serial interval distribution estimated in Leung *et al.* (*45*) (i.e., Gamma distribution with

mean and standard deviation of 5.2 and 1.7 days). The inference framework incorporates both incidence and genotype frequency data that reflect the local comparative transmissibility of cocirculating lineages.

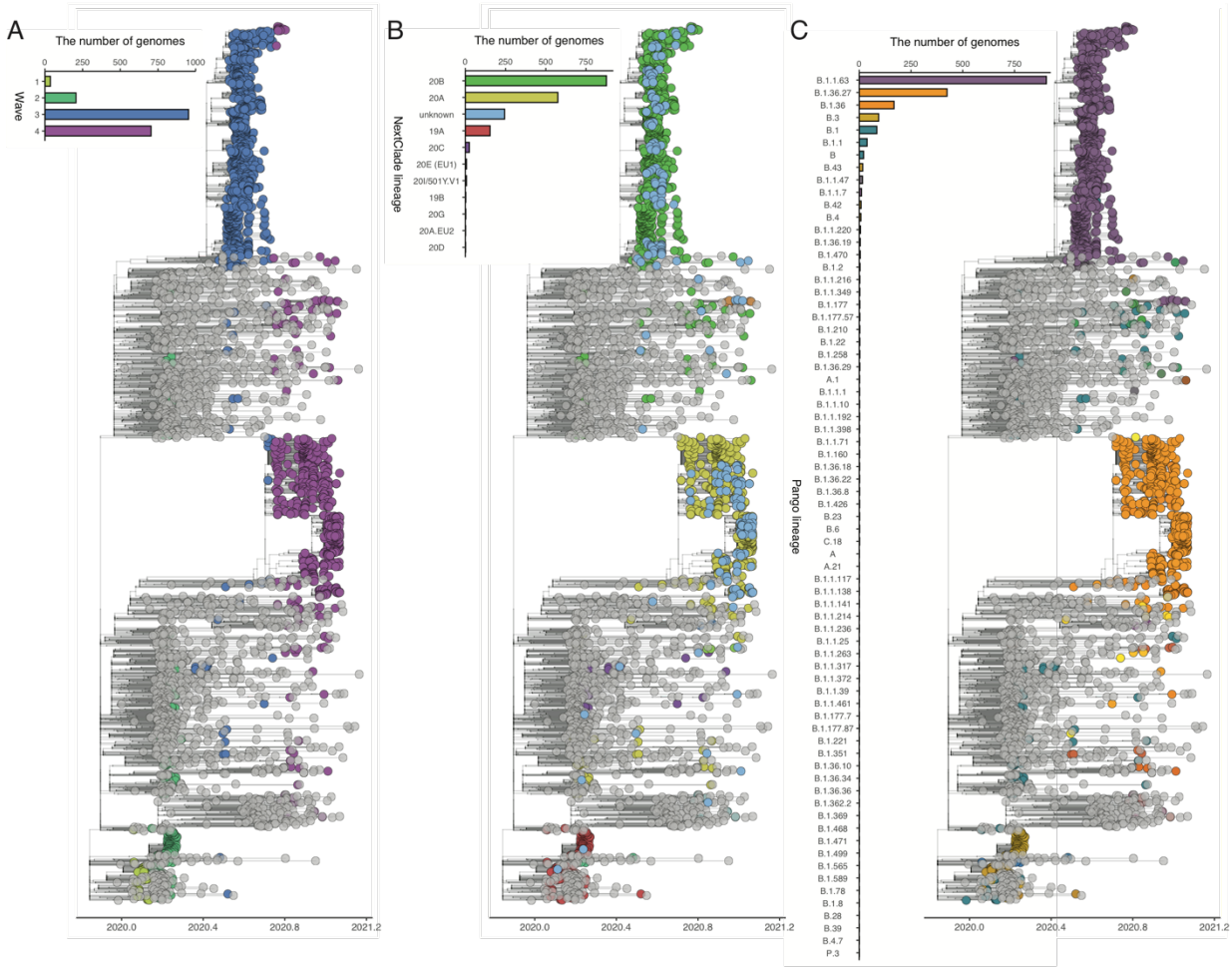

Fig. S1.

Time-scaled maximum-likelihood phylogeny of SARS-CoV2 using IQ-TREE (v.2) (*26*). The tree colored by (**A**) pandemic waves in Hong Kong, (**B**) Nextclade, and (**C**) PANGO classification, respectively. Global sequences are shown in grey.

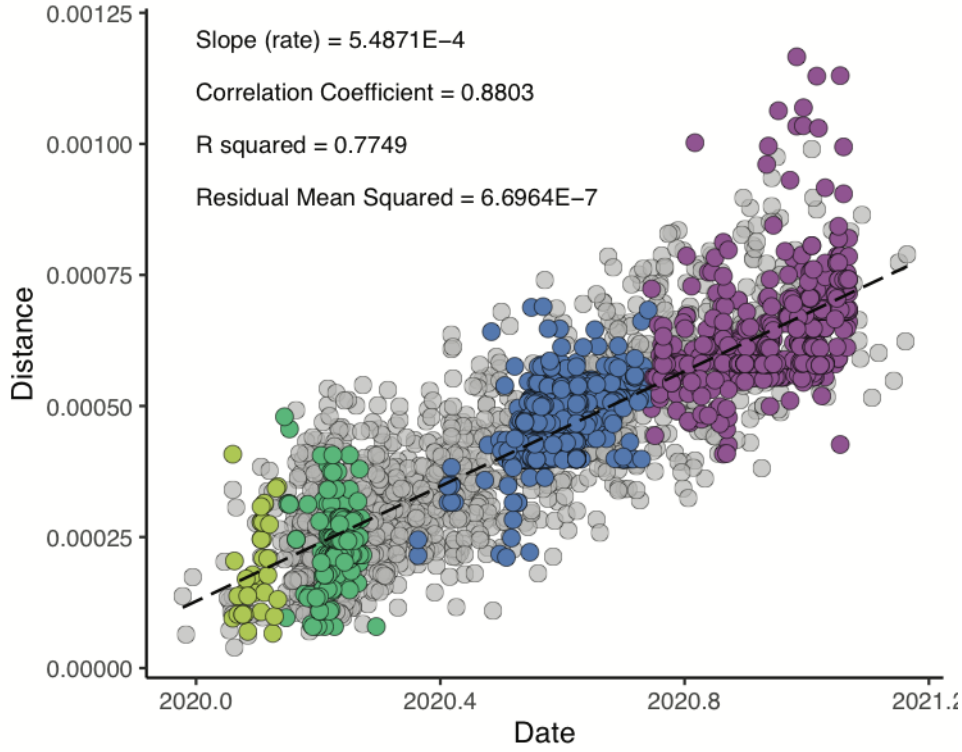

Fig. S2.

Root-to-tip regression analysis was performed in TempEst v.1.5.3 (*25*). Colours indicate pandemic waves in Hong Kong as in **fig. S1 (A)**.

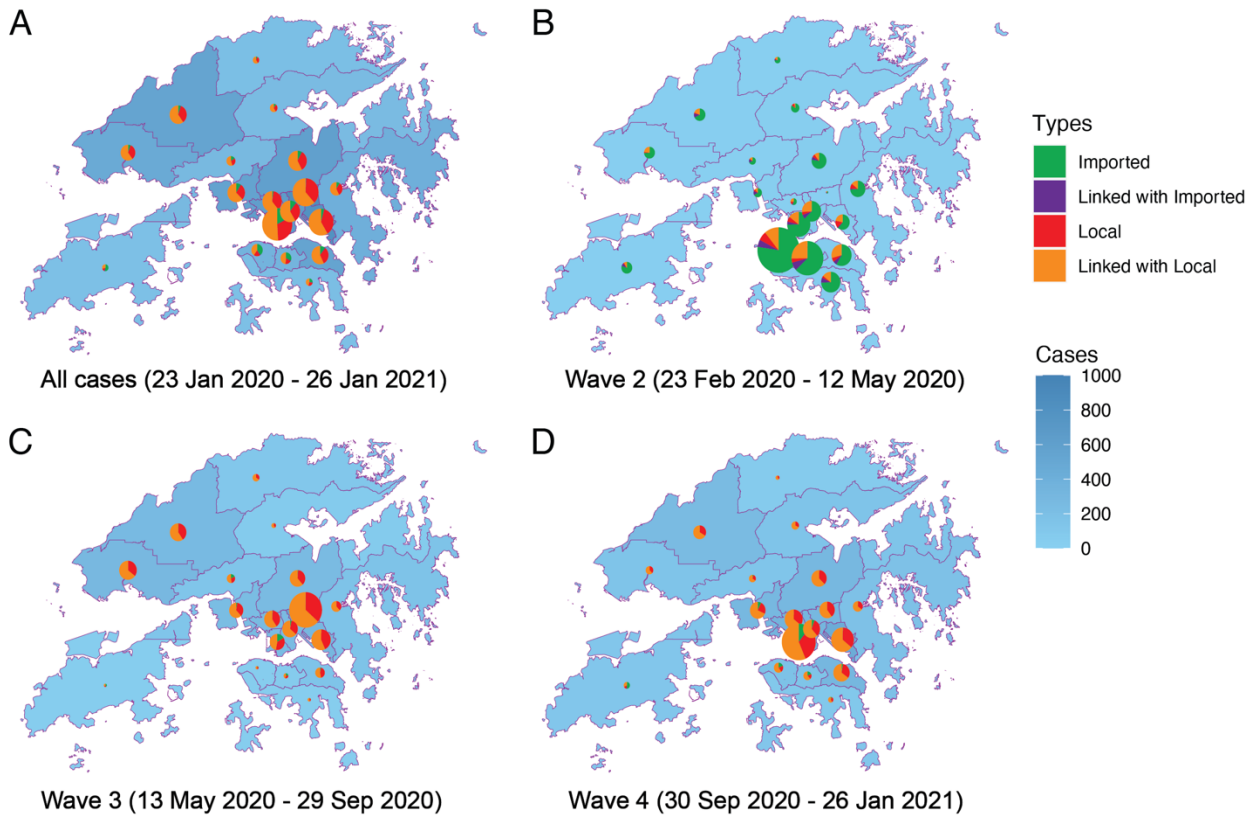

Fig. S3.

Geography of SARS-CoV-2 cases in Hong Kong. (**A**) Map of Hong Kong's 18 districts shaded by the number of laboratory-confirmed cases of SARS-CoV-2. Pie charts divided by transmission types. Pie chart size reflects the number of laboratory-confirmed cases in this district (ratio of cases and radius: 1/50,000). (**B**) same as (**A**) based on second wave (ratio of cases and radius in pie charts: 1/5,000). (**C**) same as (**A**) based on third wave (ratio of cases and radius in pie charts: 1/25,000). (**D**) same as (**A**) based on fourth wave (ratio of cases and radius in pie charts: 1/30,000).

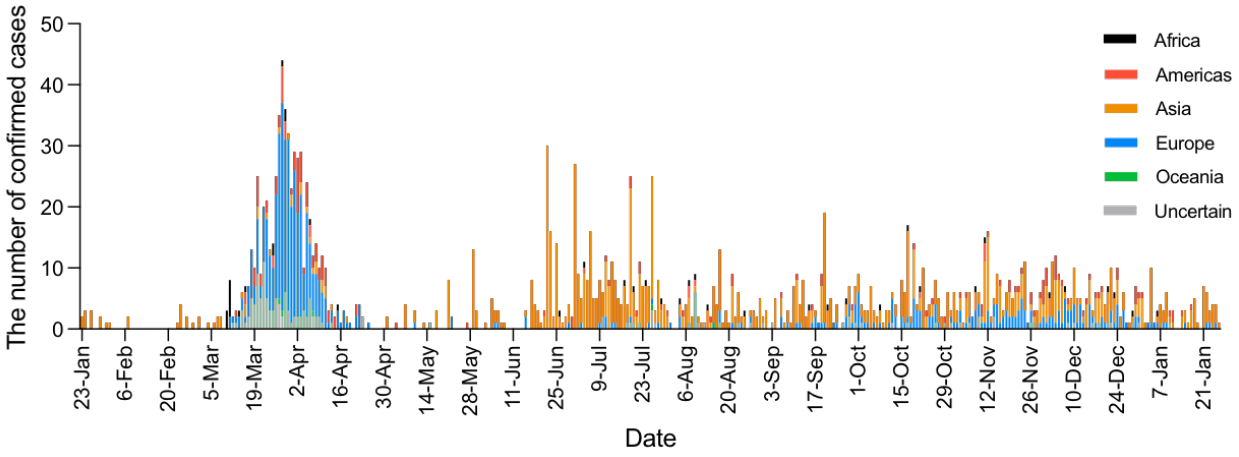

Fig. S4.

SARS-CoV-2 imported cases colored by continent of origin.

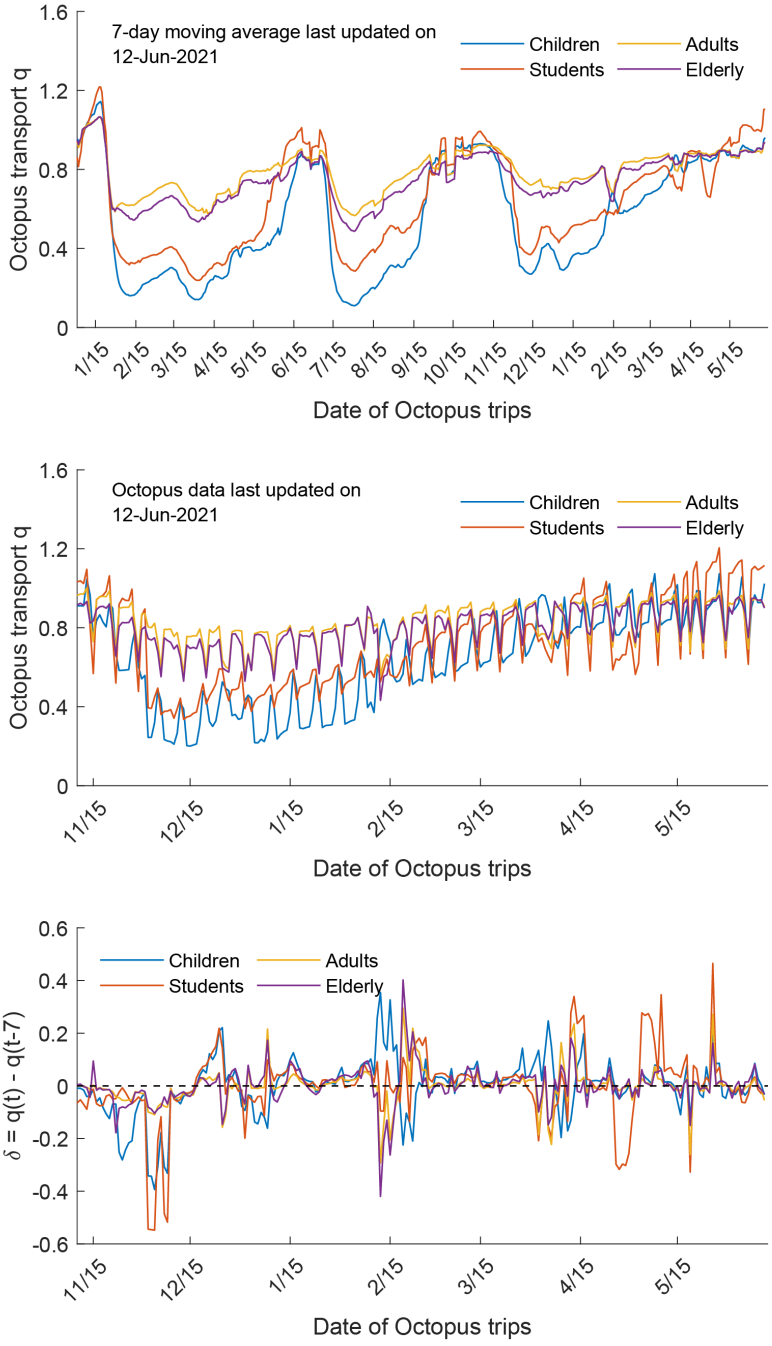

Fig. S5.
Octopus mobility data during pre-pandemic period and early period of wave four in Hong Kong.

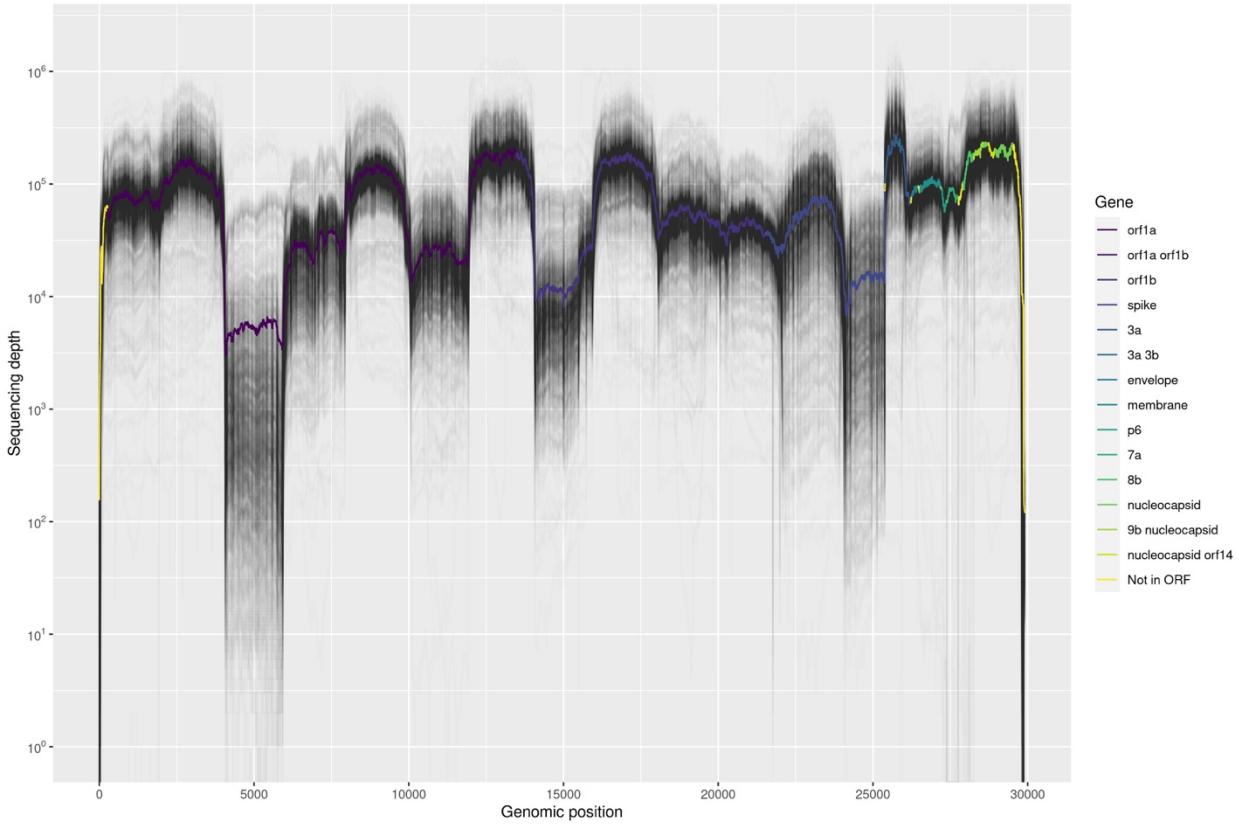

Fig. S6.
Sequencing depth of NGS data across the genome. The colored line represents the average read depth at each genomic position.

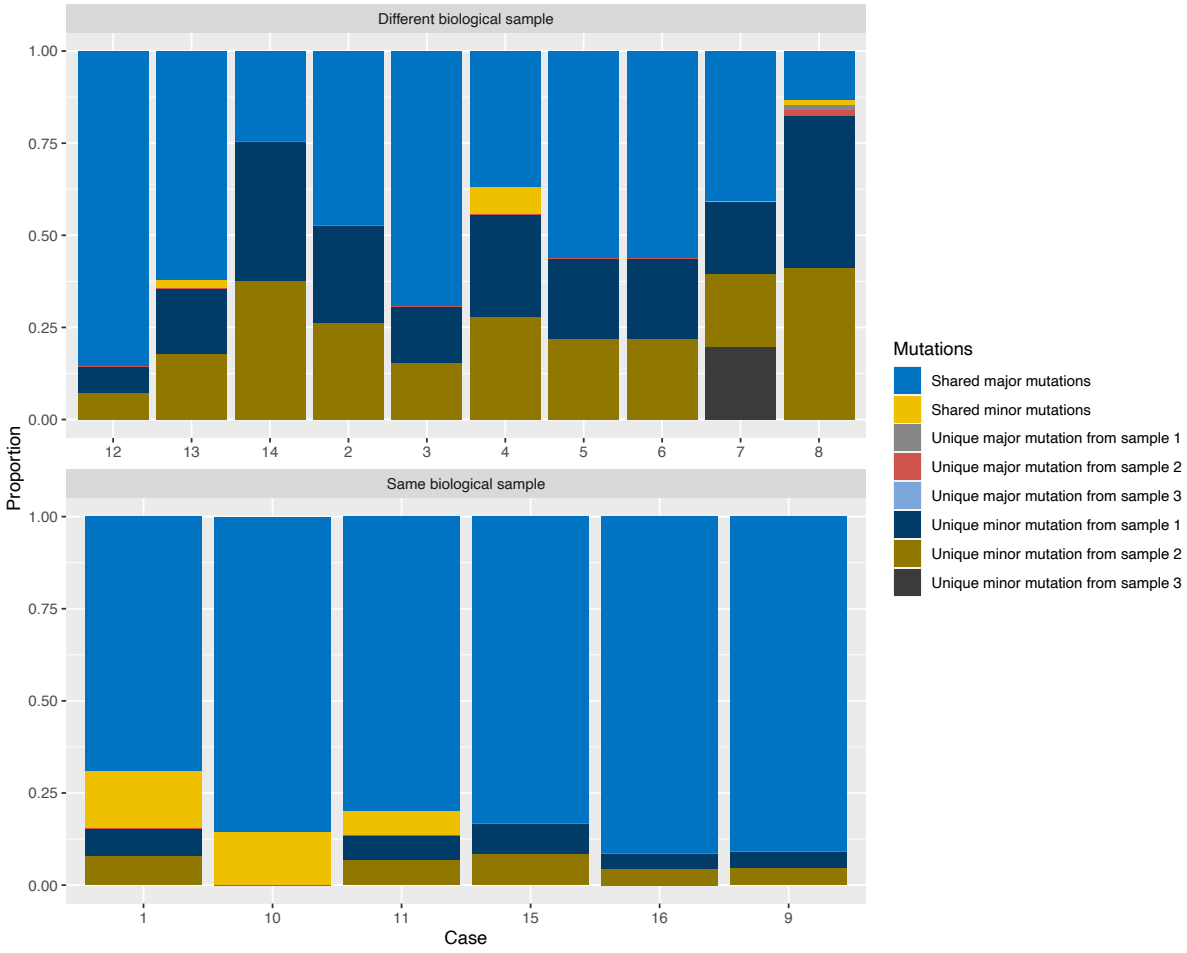

Fig. S7.
Proportion of shared mutations between samples from same individuals.

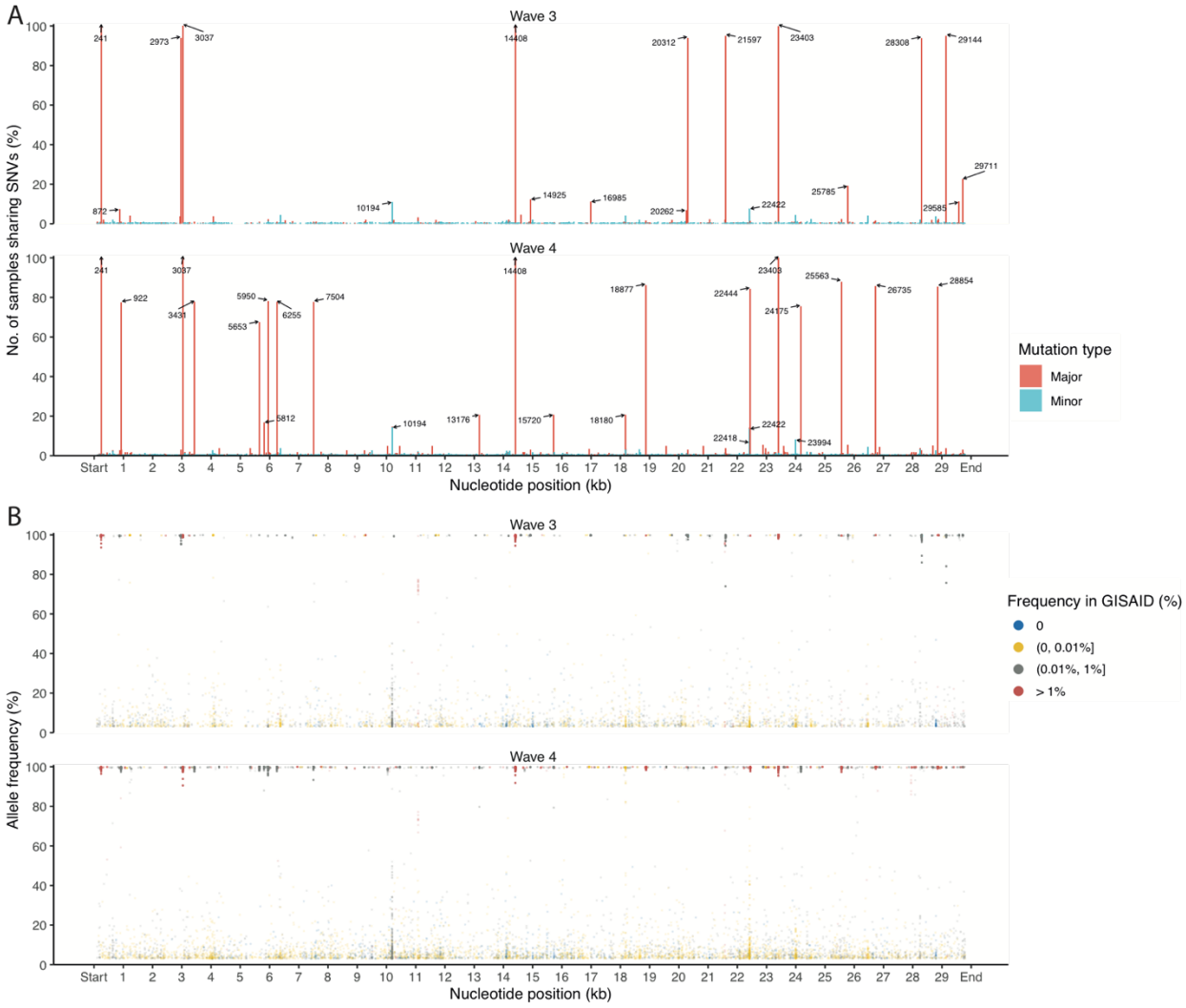

Fig. S8.
Frequencies and dynamics of SNVs in Hong Kong. (**A**) Percentage of samples that share mutations in third and fourth wave epidemics. The color codes for major and minor mutations at different genomic sites. High-frequency variant sites (n = 36, identified in at least 5% of the respective samples) are labeled. (**B**) Relative mutation frequency (allele frequency) of SNVs. The SNVs are colored by the frequencies of mutations reported in GISIAD dataset.

Table S1.
Cases and genome sequences from waves of SARS-CoV-2 in Hong Kong.

Wave	Duration	Peak of wave (no. of cases on peak day)	Travel-related cases [b]	Community cases [c]	Total confirmed cases	Genomes sequenced	Changes in stringency [d]
1	23-Jan to 22-Feb	9-Feb (10 cases)	17	53	70	36	1-2-3
2	23-Feb to 12-May	27-Mar (65 cases)	705	273	978	206	3-2-3-4
3	13-May to 29-Sep	30-Jul (149 cases)	647	3385	4032	953	4-3-2-4-3
4[a]	30-Sep to 26-Jan 2021	29-Nov (115 cases)	629	4515	5144	704	3-4-5

[a]wave four is summarized until 26 Jan 2021 for this study. [b] imported cases only. [c] epidemiologically linked with imported cases, local cases, and epidemiologically linked with local cases. [d]A-B denotes the stringency index level (based on Oxford COVID-19 Government Response Tracker, See Methods) change from A to B (e.g., 1-2-3 means that the stringency index level was increased from 1 to 2 to 3.

Table S2.
Genome sequencing and population statistics of Hong Kong districts.

Districts	SARS-COV-2 sample size [a]	Sequenced [b]	Latitude [c]	Longitude [c]	Population size [d]	Population density [d] (people per km^2)	Median monthly household income [d] (HK$)
Central and Western	365	58	22.282150	114.156880	240,500	19,171	41,400
Eastern	548	81	22.284030	114.224220	545,600	30,336	34,300
Southern	219	42	22.246760	114.174134	264,600	6,812	32,800
Wan Chai	348	76	22.279680	114.171680	178,400	16,973	44,100
Sham Shui Po	626	126	22.330700	114.162163	416,500	44,517	24,300
Kowloon City	646	140	22.328290	114.191490	419,900	41,919	30,000
Kwun Tong	804	153	22.313260	114.225810	688,500	61,075	22,500
Wong Tai Sin	841	132	22.342140	114.195830	416,100	44,729	25,500
Yau Tsim Mong	977	216	22.321320	114.172580	329,900	47,177	30,000
Islands	203	38	22.210370	114.028800	186,500	1,054	28,400
Kwai Tsing	566	124	22.354880	114.084010	502,400	21,528	24,700
North	207	43	22.494711	114.138123	314,100	2,301	30,400
Sai Kung	400	78	22.381540	114.270393	472,500	3,645	36,500
Sha Tin	601	99	22.387159	114.195229	688,100	10,014	29,700
Tai Po	246	50	22.450840	114.164223	306,800	2,254	25,800
Tsuen Wan	288	66	22.374630	114.115097	311,800	5,034	32,600
Tuen Mun	473	127	22.396910	113.974411	495,100	5,964	25,000
Yuen Long	553	134	22.445570	114.022293	645,000	4,711	27,000

[a] There are 1313 cases that have unknown location information. [b] There are 116 genomes that have unknown location information. [c] Data from https://www.latlong.net/. [d] Data from the Census and Statistics Department (Hong Kong) in 2019.

Table S3.
Travel related cases and epidemiologically linked with imported cases within seven Hong Kong monophyletic clades (over 10 community cases).

The number of samples within lineage	Travel related case ID	Report date	District	Origin [a]
902	349	2020-07-15	Unknown	Philippines
	1156	2020-09-11	Unknown	Philippines
	783	2020-08-02	Eastern	Philippines
552	1180	2020-09-20	Kowloon City	Nepal
	1182	2020-09-20	Yau Tsim Mong	Nepal
	1209	2020-10-05	Yau Tsim Mong	Nepal
	1183	2020-09-20	Yau Tsim Mong	Nepal
	1211	2020-10-06	Yau Tsim Mong	Nepal
	1203	2020-10-04	Yau Tsim Mong	Nepal
	1208	2020-10-05	Yau Tsim Mong	Nepal
	1184	2020-09-20	Yau Tsim Mong	Nepal
	1181	2020-09-20	Kowloon City	Nepal
92	NA[a]			
33	1596	2020-12-24	Central and Western	United Kingdom
	1591	2020-12-22	Wan Chai	United Kingdom
	1592	2020-12-23	Yau Tsim Mong	India
	1593	2020-12-23	Yau Tsim Mong	India
	1590	2020-12-22	Wan Chai	India
	1586	2020-12-21	NA	India
29	84	2020-03-21	Yuen Long	United Kingdom
	91	2020-03-22	Tsuen Wan	United Kingdom
	81	2020-03-20	Eastern	United Kingdom
	68	2020-03-18	Shatin	United Kingdom
	78	2020-03-20	Eastern	United Kingdom
	111	2020-03-24	Central and Western	United Kingdom
	93	2020-03-22	Eastern	United Kingdom
	92	2020-03-22	Eastern	United Kingdom
	77	2020-03-20	Kwai Tsing	United Kingdom
	71	2020-03-20	Central and Western	United Kingdom
	90	2020-03-22	Tsuen Wan	United Kingdom
	82	2020-03-20	Shatin	United Kingdom
	83	2020-03-21	Yuen Long	United Kingdom
19	NA[b]			
16	256	2020-07-01	Shatin	United States of America

[a] This result is based on epidemiological data. [b] No travel-related cases.

Table S4.
Distribution of PANGO lineages across HK-wave3 and HK-wave4A clades.

HK clade	PANGO lineage	Number of genomes
HK-wave3	B.1.1.63	888
	B.1.1	5
	B.1.1.220	6
	B.1.1.192	2
	B.1.1.398	1
HK-wave4A	B.1.36.27	424
	B.1.36	124
	B.1.36.29	2
	B.1.36.10	1
	B.1.36.34	1

Table S5.

Sample numbers associated with different transmission settings in HK-wave3, HK-wave4A and all community cases in wave3 and wave4 based on epidemiological data.

Transmission setting	Wave3 community cases (epidemiological data)	Wave4 community cases (epidemiological data)	HK-wave3 clade (sequenced data)	HK-wave4A clade (sequenced data)
Social	408	802	114	130
Rche/Rchd [a]	145	117	47	4
Family/Roommate	1800	2352	470	226
Unknown/Sporadic	661	763	149	84
Work	354	421	118	81
Nosocomial	17	60	4	27

[a] Residential care homes for the elderly and disabled.

Table S6.
Major SNVs identified in third and fourth waves in Hong Kong.

Position	Wave	Gene	Synonymous mutation	Mutation at nucleotide	Mutation at amino acid	Number of samples with major SNVs	Number of samples with iSNVs	Frequency in GISAID	Proportion in GISAID (%)
241	Wave 3 & 4	Not in ORF	Not in ORF	C241T	NA	1598	0	377531	94.59
3037	Wave 3 & 4	nsp3	TRUE	C3037T	F106F	1600	0	381081	95.48
10194	Wave 3 & 4	nsp5	FALSE	A10194T|G	E47V|G	2	392	43	0.01
14408	Wave 3 & 4	nsp12_2	FALSE	C14408T	P314L	1595	0	380926	95.44
22422	Wave 3 & 4	S	FALSE	A22422G|T	D287G|V	5	322	28	0.01
23403	Wave 3 & 4	S	FALSE	A23403G	D614G	1597	0	381443	95.57
872	Wave 3	nsp2	FALSE	G872A|T|C	D23N|Y|H	82	4	679	0.17
2973	Wave 3	nsp3	FALSE	C2973T	A85V	859	1	1500	0.38
14925	Wave 3	nsp12_2	TRUE	C14925T	V486V	128	0	849	0.21
16985	Wave 3	nsp13	FALSE	C16985T	T250I	98	1	141	0.04
20262	Wave 3	nsp15	TRUE	A20262G	L214L	60	1	522	0.13
20312	Wave 3	nsp15	FALSE	C20312T	A231V	859	0	148	0.04
21597	Wave 3	S	FALSE	C21597T	S12F	874	1	633	0.16
25785	Wave 3	ORF3a	FALSE	G25785T|A	W131C|*	202	8	1864	0.47
28308	Wave 3	N	FALSE	C28308G|T	A12G|V	857	1	160	0.04
29144	Wave 3	N	TRUE	C29144T	L291L	874	0	606	0.15
29585	Wave 3	ORF10	FALSE	C29585T	P10S	97	2	701	0.18
29711	Wave 3	Not in ORF	Not in ORF	G29711T	NA	220	0	596	0.15
922	Wave 4	nsp2	TRUE	G922A	L39L	549	0	223	0.06
3431	Wave 4	nsp3	FALSE	G3431T	V238L	552	0	426	0.11
5653	Wave 4	nsp3	TRUE	T5653C	Y978Y	479	0	109	0.03
5812	Wave 4	nsp3	TRUE	C5812T	D1031D	117	1	903	0.23
5950	Wave 4	nsp3	FALSE|TRUE	G5950T|A	K1077N|K	1110	12	1175	0.29
6255	Wave 4	nsp3	FALSE	C6255T	A1179V	552	0	543	0.14
7504	Wave 4	nsp3	TRUE	C7504T	Y1595Y	551	0	170	0.04
13176	Wave 4	nsp10	FALSE	C13176T	T51I	144	0	235	0.06
15720	Wave 4	nsp12_2	TRUE	C15720T	D751D	144	3	1377	0.35
18180	Wave 4	nsp14	TRUE	G18180A	K47K	144	0	33	0.01
18877	Wave 4	nsp14	TRUE	C18877T	L280L	617	1	23681	5.93
22418	Wave 4	S	FALSE	A22418G	T286A	1	76	1	0
22444	Wave 4	S	TRUE	C22444T	D294D	603	1	7893	1.98
23994	Wave 4	S	FALSE	A23994G	K811R	1	93	9	0
24175	Wave 4	S	TRUE	T24175C	A871A	536	0	59	0.01
25563	Wave 4	ORF3a	FALSE	G25563C|T	Q57H	631	10	89470	22.42
26735	Wave 4	M	TRUE	C26735T	Y71Y	614	1	21029	5.27
28854	Wave 4	N	FALSE	C28854T	S194L	611	3	23575	5.91

Table S7.
Minor SNVs identified in Hong Kong cases (frequency in GISAID ≥1%).

Position	Gene	Frequency in HK	(%)	Silent mutation	Frequency in GISAID	Frequency in GISAID (%)	Mutation (nucleotide)	Mutation (amino acid)
28883	N	25	1.56	FALSE	152044	38.09	G28883C	G610R
26801	M	10	0.62	TRUE	86175	21.59	C26801G|T	L279L
22227	S	11	0.69	FALSE	85789	21.49	C22227T	A665V
21255	nsp16	9	0.56	TRUE	85524	21.43	G21255T|C	A597A
6286	nsp3	12	0.75	TRUE	85407	21.4	C6286T	T3567T
29645	ORF10	10	0.62	FALSE	85145	21.33	G29645T	V88L
28932	N	9	0.56	FALSE	85057	21.31	C28932A|T	A659D|V
445	nsp1	10	0.62	TRUE	84963	21.29	T445C	V180V
1059	nsp2	13	0.81	FALSE	59725	14.96	C1059T	T254I
27944	ORF8	7	0.44	TRUE	57276	14.35	C27944T	H51H
23604	S	15	0.94	FALSE	56514	14.16	C23604T|G|A	P2042L|R|H
23063	S	16	1	FALSE	53756	13.47	A23063T|G	N1501Y|D
5986	nsp3	13	0.81	TRUE	53506	13.41	C5986T	F3267F
28977	N	16	1	FALSE	53437	13.39	C28977T	S704F
3267	nsp3	18	1.12	FALSE	52970	13.27	C3267T	T548I
14676	nsp12_2	12	0.75	TRUE	52930	13.26	C14676T	P1209P
23709	S	11	0.69	FALSE	52646	13.19	C23709T	T2147I
27972	ORF8	12	0.75	FALSE	52586	13.18	C27972T	Q79*
24914	S	12	0.75	FALSE	52551	13.17	G24914T|C	D3352Y|H
15279	nsp12_2	12	0.75	TRUE	52500	13.15	C15279T	H1812H
23271	S	11	0.69	FALSE	52472	13.15	C23271A	A1709D
28048	ORF8	12	0.75	FALSE	52430	13.14	G28048A|T	R155K|I
24506	S	11	0.69	FALSE	52370	13.12	T24506G	S2944A
16176	nsp12_2	12	0.75	TRUE	52366	13.12	T16176C	T2709T
28111	ORF8	10	0.62	FALSE	52347	13.12	A28111G	Y218C
6954	nsp3	11	0.69	FALSE	52344	13.11	T6954C	I4235T
5388	nsp3	7	0.44	FALSE	52288	13.1	C5388A	A2669D
913	nsp2	14	0.87	TRUE	52196	13.08	C913T	S108S
204	Not in ORF	5	0.31	Not in ORF	47971	12.02	G204T|A	NA
21614	S	4	0.25	FALSE	39312	9.85	C21614T	L52F
20268	nsp15	7	0.44	TRUE	26684	6.69	A20268G	L648L
27964	ORF8	6	0.37	FALSE	24942	6.25	C27964T	S71L
28869	N	7	0.44	FALSE	23983	6.01	C28869T	P596L
313	nsp1	24	1.5	TRUE	21829	5.47	C313T	L48L
22992	S	9	0.56	FALSE	21826	5.47	G22992C|A|T	S1430T|N|I
10319	nsp5	6	0.37	FALSE	20462	5.13	C10319T|A	L265F|I
11083	nsp6	38	2.37	FALSE|TRUE	20168	5.05	G11083T|A	L111F|L
17615	nsp13	9	0.56	FALSE	19741	4.95	A17615G	K1379R
28975	N	5	0.31	FALSE	19390	4.86	G28975C|T|A	M702I
21304	nsp16	6	0.37	FALSE	18702	4.69	C21304T	R646C
18424	nsp14	4	0.25	FALSE	17916	4.49	A18424G	N385D
25907	ORF3a	4	0.25	FALSE	17673	4.43	G25907T	G515V
28472	N	4	0.25	FALSE	17473	4.38	C28472T	P199S
14805	nsp12_2	4	0.25	TRUE	14592	3.66	C14805T	Y1338Y
4543	nsp3	5	0.31	TRUE	11630	2.91	C4543T	T1824T
25710	ORF3a	3	0.19	TRUE	11496	2.88	C25710T	L318L
15766	nsp12_2	2	0.12	FALSE	11473	2.87	G15766T	V2299L
17019	nsp13	5	0.31	FALSE|TRUE	11208	2.81	G17019T|A	E783D|E
9526	nsp4	4	0.25	FALSE	11146	2.79	G9526T|C	M972I
13993	nsp12_2	2	0.12	FALSE	11064	2.77	G13993T	A526S
11497	nsp6	2	0.12	TRUE	11042	2.77	C11497T	Y525Y

26876	M	2	0.12	TRUE	10983	2.75	T26876C	I354I
16889	nsp13	2	0.12	FALSE	10934	2.74	A16889G	K653R
29399	N	2	0.12	FALSE	10916	2.73	G29399A	A1126T
23401	S	3	0.19	FALSE	10620	2.66	G23401T	Q1839H
5629	nsp3	2	0.12	TRUE	10398	2.61	G5629T	T2910T
15324	nsp12_2	4	0.25	TRUE	10168	2.55	C15324T	N1857N
29734	Not in ORF	5	0.31	Not in ORF	9939	2.49	G29734T|C	NA
222	Not in ORF	2	0.12	Not in ORF	9834	2.46	C222T	NA
17104	nsp13	5	0.31	FALSE	8996	2.25	C17104T	H868Y
22879	S	3	0.19	FALSE	8965	2.25	C22879A	N1317K
29366	N	3	0.19	FALSE	8923	2.24	C29366T	P1093S
7767	nsp3	12	0.75	FALSE	8618	2.16	T7767C	I5048T
8047	nsp3	3	0.19	TRUE	8583	2.15	C8047T	Y5328Y
8083	nsp3	5	0.31	FALSE	8156	2.04	G8083A	M5364I
20661	nsp16	3	0.19	TRUE	8129	2.04	T20661C	S3S
29402	N	10	0.62	FALSE	7511	1.88	G29402T|C	D1129Y|H
27800	ORF7b	3	0.19	TRUE	7440	1.86	C27800A	A39A
28725	N	3	0.19	FALSE	7311	1.83	C28725T	P452L
9286	nsp4	17	1.06	TRUE	7271	1.82	C9286T	N732N
10097	nsp5	6	0.37	FALSE	6822	1.71	G10097A|T|C	G43S|C|R
18028	nsp13	6	0.37	FALSE	6674	1.67	G18028T	A1792S
21855	S	5	0.31	FALSE	6653	1.67	C21855T	S293F
21575	S	25	1.56	FALSE	6592	1.65	C21575T	L13F
12988	nsp9	5	0.31	FALSE	6563	1.64	G12988T|C	M303I
26972	M	3	0.19	TRUE	6559	1.64	T26972C	R450R
15598	nsp12_2	3	0.19	FALSE	6554	1.64	G15598A	V2131I
24910	S	5	0.31	TRUE	6544	1.64	T24910C|G	T3348T
2453	nsp2	4	0.25	FALSE	6270	1.57	C2453T	L1648F
28651	N	4	0.25	TRUE	6143	1.54	C28651T	N378N
28887	N	8	0.5	FALSE	6124	1.53	C28887T	T614I
19839	nsp15	2	0.12	TRUE	6093	1.53	T19839C	N219N
23731	S	4	0.25	TRUE	6068	1.52	C23731T	T2169T
10323	nsp5	11	0.69	FALSE	5911	1.48	A10323G	K269R
11396	nsp6	3	0.19	FALSE	5509	1.38	C11396T	L424F
2416	nsp2	6	0.37	TRUE	5362	1.34	C2416T	Y1611Y
10870	nsp5	5	0.31	TRUE	5156	1.29	G10870T|A	L816L
9745	nsp4	3	0.19	TRUE	5069	1.27	C9745T	Y1191Y
20451	nsp15	4	0.25	TRUE	4978	1.25	C20451T	N831N
22346	S	4	0.25	FALSE	4665	1.17	G22346T	A784S
28087	ORF8	2	0.12	FALSE	4662	1.17	C28087T	A194V
26424	E	7	0.44	TRUE	4656	1.17	T26424C	S180S
8603	nsp4	3	0.19	FALSE	4626	1.16	T8603C	F49L
13536	nsp12_2	3	0.19	TRUE	4547	1.14	C13536T	Y69Y
15480	nsp12_2	3	0.19	TRUE	4530	1.13	C15480A|T	T2013T
3177	nsp3	3	0.19	FALSE	4398	1.1	C3177T	P458L
8917	nsp4	8	0.5	TRUE	4375	1.1	C8917T	F363F
4002	nsp3	4	0.25	FALSE	4288	1.07	C4002T	T1283I
19524	nsp14	3	0.19	TRUE	4175	1.05	C19524T	L1485L
29179	N	5	0.31	TRUE	4162	1.04	G29179T|A|C	P906P
25437	ORF3a	4	0.25	FALSE	4088	1.02	G25437T	L45F
22388	S	2	0.12	TRUE	4038	1.01	C22388T	L826L
28253	ORF8	43	2.69	TRUE	3982	1	C28253T	F360F

Table S8.
Estimation on bottleneck size of transmission pairs.

Transmission pair	Variant calling threshold	Donor	Recipient	Bottleneck size	CI lower	CI upper
Cluster_fam_1122	0.03	8773	8772	3	1	10
Cluster_fam_1166	0.03	9042	9041	2	1	4
Cluster_fam_197	0.03	1905	2168	1	0	9
Cluster_fam_222	0.03	2172	2317	1	0	27
Cluster_fam_293	0.03	2735	2609	1	0	202
Cluster_fam_336	0.03	2989	2962	1	0	13
Cluster_fam_509	0.03	3970	3612	1	0	22
Cluster_fam_562	0.03	4306	4307	NA	NA	NA
Cluster_fam_718	0.03	5399	5444	1	0	13
Cluster_fam_730	0.03	5539	5577	NA	NA	NA
Cluster_friends_25	0.03	1839	2047	1	0	10
Cluster_roommate_08	0.03	2721	2545	1	0	5
Cluster_roommate_21	0.03	4075	4208	1	0	4

Table S9.

Highly shared variant sites (allele frequency ≥3% and were found in >1% of the HK samples) located within or related to PCR primer binding regions.

Position	Number of samples with SNV	Proportion in HK samples
1912	18	0.01124297
1947	551	0.3441599
15487	28	0.01748907
15489	1105	0.69019363
15494	1151	0.71892567
18100	347	0.21673954
24082	178	0.11118051
24091	860	0.53716427
26060	550	0.34353529
29799	21	0.0131168

Table S10.
Gene annotation of SARS-CoV-2 Genome (nucleotide positions base on reference sequence Wuhan-Hu-1, GenBank: MN908947.3).

Gene segment	Start	Stop
nsp1	266	805
nsp2	806	2719
nsp3	2720	8554
nsp4	8555	10054
nsp5	10055	10972
nsp6	10973	11842
nsp7	11843	12091
nsp8	12092	12685
nsp9	12686	13024
nsp10	13025	13441
nsp12_1	13442	13468
nsp12_2	13468	16236
nsp13	16237	18039
nsp14	18040	19620
nsp15	19621	20658
nsp16	20659	21555
S	21563	25384
ORF3a	25393	26220
E	26245	26472
M	26523	27191
ORF6	27202	27387
ORF7a	27394	27753
ORF7b	27762	27887
ORF8	27894	28259
N	28274	29533
ORF10	29558	29674

Data S1. (Data S1.csv)

Origins of imported cases in Hong Kong.

Data S2. (Data S2.csv)

Sample list with waves, NextClade and PANGO lineage designations.

Data S3. (Data S3.csv)

Summary of Hong Kong monophyletic clades.

Data S4. (Data S4.pdf)

Acknowledgements to sequences obtained from GISAID (accessed on 11-June-2021).

Supplementary references

22. T. H. C. Sit *et al.*, Infection of dogs with SARS-CoV-2. *Nature* **586**, 776-778 (2020).
23. M. Vasimuddin, S. Misra, H. Li, S. Aluru, in *2019 IEEE International Parallel and Distributed Processing Symposium (IPDPS)*. (2019), pp. 314-324.
24. H. Li, A statistical framework for SNP calling, mutation discovery, association mapping and population genetical parameter estimation from sequencing data. *Bioinformatics* **27**, 2987-2993 (2011).
25. A. Rambaut, T. T. Lam, L. Max Carvalho, O. G. Pybus, Exploring the temporal structure of heterochronous sequences using TempEst (formerly Path-O-Gen). *Virus Evol* **2**, vew007 (2016).
26. L. T. Nguyen, H. A. Schmidt, A. von Haeseler, B. Q. Minh, IQ-TREE: a fast and effective stochastic algorithm for estimating maximum-likelihood phylogenies. *Mol Biol Evol* **32**, 268-274 (2015).
27. T. H. To, M. Jung, S. Lycett, O. Gascuel, Fast Dating Using Least-Squares Criteria and Algorithms. *Syst Biol* **65**, 82-97 (2016).
28. L. du Plessis *et al.*, Establishment and lineage dynamics of the SARS-CoV-2 epidemic in the UK. *Science* **371**, 708-712 (2021).
29. S. Duchene *et al.*, Temporal signal and the phylodynamic threshold of SARS-CoV-2. *Virus Evol* **6**, veaa061 (2020).
30. A. J. Drummond, A. Rambaut, B. Shapiro, O. G. Pybus, Bayesian coalescent inference of past population dynamics from molecular sequences. *Mol Biol Evol* **22**, 1185-1192 (2005).
31. J. L. Geoghegan *et al.*, Genomic epidemiology reveals transmission patterns and dynamics of SARS-CoV-2 in Aotearoa New Zealand. *Nat Commun* **11**, 6351 (2020).
32. S. Y. Ho, S. Duchene, D. Duchene, Simulating and detecting autocorrelation of molecular evolutionary rates among lineages. *Mol Ecol Resour* **15**, 688-696 (2015).
33. R. Bouckaert *et al.*, BEAST 2.5: An advanced software platform for Bayesian evolutionary analysis. *PLoS Comput Biol* **15**, e1006650 (2019).
34. A. J. Drummond, S. Y. Ho, M. J. Phillips, A. Rambaut, Relaxed phylogenetics and dating with confidence. *Plos Biol* **4**, e88 (2006).
35. A. Rambaut, A. J. Drummond, D. Xie, G. Baele, M. A. Suchard, Posterior Summarization in Bayesian Phylogenetics Using Tracer 1.7. *Syst Biol* **67**, 901-904 (2018).
36. E. P. Garrison, G. Marth, Haplotype-based variant detection from short-read sequencing. *arXiv: Genomics*, (2012).
37. Z. Lai *et al.*, VarDict: a novel and versatile variant caller for next-generation sequencing in cancer research. *Nucleic Acids Res* **44**, e108 (2016).
38. A. Wilm *et al.*, LoFreq: a sequence-quality aware, ultra-sensitive variant caller for uncovering cell-population heterogeneity from high-throughput sequencing datasets. *Nucleic Acids Res* **40**, 11189-11201 (2012).
39. K. M. Gostic *et al.*, Practical considerations for measuring the effective reproductive number, Rt. *PLoS Comput Biol* **16**, e1008409 (2020).
40. J. T. Wu *et al.*, Nowcasting epidemics of novel pathogens: lessons from COVID-19. *Nat Med* **27**, 388-395 (2021).
41. J. A. Backer, D. Klinkenberg, J. Wallinga, Incubation period of 2019 novel coronavirus (2019-nCoV) infections among travellers from Wuhan, China, 20-28 January 2020. *Euro Surveill* **25**, (2020).

42. R. N. Thompson *et al.*, Improved inference of time-varying reproduction numbers during infectious disease outbreaks. *Epidemics* **29**, 100356 (2019).
43. K. Leung, M. Lipsitch, K. Y. Yuen, J. T. Wu, Monitoring the fitness of antiviral-resistant influenza strains during an epidemic: a mathematical modelling study. *Lancet Infect Dis* **17**, 339-347 (2017).
44. K. Leung, Y. Pei, G. M. Leung, T. T. Lam, J. T. Wu, Empirical transmission advantage of the D614G mutant strain of SARS-CoV-2. *medRxiv*, (2020).
45. K. Leung, J. T. Wu, D. Liu, G. M. Leung, First-wave COVID-19 transmissibility and severity in China outside Hubei after control measures, and second-wave scenario planning: a modelling impact assessment. *Lancet* **395**, 1382-1393 (2020).